Optically tunable bianisotropy in a sphere made from an epsilon-near-zero material

Mahmoud A. A. Abouelatta,[1] Akbar Safari,[2] M. Zahirul Alam,[2,3] Xavier Garcia-Santiago,[4] Dominik Beutel,[1] Lin Cheng,[2] Robert W. Boyd,[2,3] Carsten Rockstuhl,[1,4] and Rasoul Alaee[1,2,*]

[1] Institute of Theoretical Solid State Physics, Karlsruhe Institute of Technology, 76131 Karlsruhe, Germany
[2] Department of Physics, University of Ottawa, Ottawa, ON K1N 6N5, Canada
[3] The Institute of Optics and Department of Physics and Astronomy, University of Rochester, Rochester, New York 14627, USA
[4] Institute of Nanotechnology, Karlsruhe Institute of Technology, 76131 Karlsruhe, Germany
*Corresponding author: rasoul.alaee@gmail.com

Bianisotropic media can be used to engineer absorbance, scattering, polarization, and dispersion of electromagnetic waves. However, the demonstration of a tunable light-induced bianisotropy at optical frequencies is still lacking. Here, we propose an experimentally feasible concept for a light-induced tunable bianisotropic response in a homogeneous sphere made of an epsilon-near-zero (ENZ) material. By exploiting the large linear absorption and the large possible intensity-dependent changes in the permittivity of ENZ materials, the direction-dependent scattering and absorption cross sections could be obtained. Our findings pave the way for further studies and applications in the optical regime requiring full dynamic control of the bianisotropic behavior.

A bianisotropic response refers to a magneto-electric coupling, accommodated in Maxwell's equations by a polarization depending on the electric and magnetic fields. Research on bianisotropic responses has increased because of the opportunities to control the scattering, absorption, and polarization of light. A bianisotropic response leads to asymmetric scattering and reflection [1], p olarization m anipulation [2], a nd asymmetric transmission [3]. Several studies showed how to obtain bianisotropic structures. A review by Asadchy *et al.* [4] distinguishes two approaches. The first is based on engineered spatial dispersion in metamaterials [1,5–8]. Here, the metamaterial's unit cell is regarded as a meta-atom with subwavelength scale details, where the magnitude and phase of the scattered field depend on the meta-atom geometry. The second approach to obtain bianisotropy is by breaking the time-reversal symmetry (reciprocity) [9–11]. Such a breaking could be achieved by schemes that rely on, e.g., externally magnetized materials [12], nonlinear materials [10], or spatiotemporally modulated materials [13].

Despite its importance, only a few concepts were suggested to achieve a tunable bianisotropy. One example is a mechanically controlled bianisotropy based on the deformation of Miura-ori patterns [14]. In another approach, the magnetic response of 3D split-ring resonators changes into a bianisotropic one by photoexciting free carriers in silicon at THz frequencies [15]. A reconfigurable bianisotropic response based on a metal-stress-driven self-folding method [16] and the rotation of three-dimensional split-ring resonators [17] were also reported. However, so far, a light-induced, reversible bianisotropic response in a homogeneous nanoparticle has not been demonstrated at optical frequencies. Here, we obtain a fast optically tunable bianisotropic response using nonlinear antennas. Our proposed scheme relies on a spherical antenna made from indium tin oxide (ITO) that possesses an effective Kerr-type nonlinearity resulting from free-electron dynamics in the conduction band of ITO. The ITO sphere is pumped with a high-intensity laser, as depicted in Fig. 1(a), at a wavelength near the epsilon-near-zero (ENZ) wavelength, where the nonlinear response becomes most pronounced. Due to the nonlinearity, the pump introduces a spatially inhomogeneous permittivity $\varepsilon(x, y, z)$ in the sphere with a broad range of values. The pump beam will break the inversion symmetry and, thus, induces a strong bianisotropic response. A low-intensity beam can then probe the scattering response of the ITO sphere. To quantify its scattering response [18], we calculate the T-matrix of the sphere. The T-matrix relates the incident optical probe beam to the scattered field. The tunable bianisotropy is qualitatively and quantitatively illustrated using the T-matrix. As a result of the optically induced bianisotropy, the scattering and absorption cross sections of the probe beam depend on the azimuthal angle (ϕ), and we study this effect computationally.

We assume an homogeneous, isotropic ITO sphere to illustrate the concept of optically induced bianisotropy. We find that the large linear optical absorption coefficient in an ITO sphere—which is typically thought to be a limiting factor for various applications—can be exploited for light-induced bianisotropy. We show that when the sphere is illuminated with a high-intensity pump (to the order of 50 GW/cm^2 or greater), the permittivity within the sphere gets spatially inhomogeneous with a large gradient. The large linear absorption in ITO [Fig. 2(a)] leads to an exponential drop of local intensity depending on the position along the direction of light propagation. Consequently,

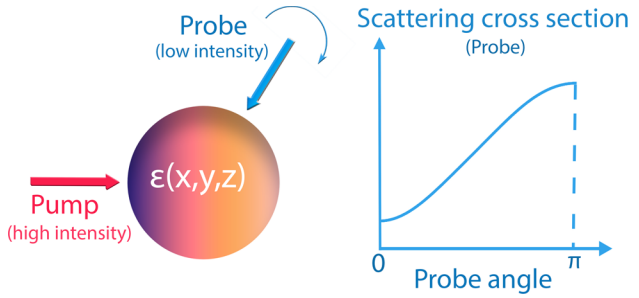

Fig. 1. Proposed optically induced bianisotropy. A high-intensity pump illuminates an ITO sphere. Owing to ITO's strong nonlinear response close to its ENZ wavelength (1240 nm), a spatially inhomogeneous permittivity is obtained, causing a bianisotropic response to a low-intensity probe. Then, the probe's scattering cross section depends on its illumination direction.

the intensity-dependent changes in local complex permittivity also exhibit a large gradient as long as the incident intensity is not too large compared with the saturation intensity. Thus, the behavior of the proposed light-induced bianisotropy stems from the interplay of linear absorption, nonlinear absorption, and large Kerr-type nonlinearity of ITO [19–21]. A bianisotropic response is obtained owing to the engineered spatial dispersion introduced by the large gradient in the sphere permittivity. As shown in Fig. 2(a), the real part of the ITO permittivity increases from near zero at very low intensities up to a saturation value of approximately 1.2 when the external pump intensity exceeds 250 GW/cm^2. This strong nonlinear response of ITO stems from the inverse proportionality between the nonlinear refractive index coefficient and the real part of the linear refractive index, which possesses a very small value at the ENZ wavelength. The nonlinear response in Fig. 2(a) is obtained by incorporating the third-, fifth-, and seventh-order nonlinear susceptibilities in the permittivity model [Eq. (1)], being a good fit to experiments [19,22,23]:

$$\varepsilon_{\mathrm{nl}}(\mathbf{r},\omega) = \varepsilon_{\mathrm{l}}(\omega) + \sum_{j=1}^{3} c_{2j+1}\chi_{eff}^{(2j+1)}(\omega)\left|\frac{\mathbf{E}(\mathbf{r},\omega)}{2}\right|^{2j}, \qquad \textbf{(1)}$$

where $\varepsilon_{\mathrm{nl}}(\mathbf{r},\omega)$, $\varepsilon_{\mathrm{l}}(\omega)$, $\chi_{eff}^{(2j+1)}(\omega)$, and $\mathbf{E}(\mathbf{r},\omega)$ denote the nonlinear permittivity, the linear permittivity, the $(2j+1)$ order of the effective nonlinear susceptibility, and the electric field value. Here, $c_3 = 3$, $c_5 = 10$, and $c_7 = 35$ are the degeneracy factors. (When the pump and probe beams are distinguishable, the degeneracy factors can be as large as $c_3 = 6$, $c_5 = 30$, and $c_7 = 140$ [24]. However, here we use more conservative values consistent with the experimental observations [19].) Owing to ITO's strong nonlinearity, the scattering, absorption, and extinction cross sections to the pump depend highly on the pump intensity itself. Therefore, the permittivity within the sphere experienced by the pump beam becomes inhomogeneous. We always choose the pump and the probe wavelengths to be 1300 and 1180 nm. Consequently, we assume that the linear permittivity is the only wavelength-dependent permittivity with values equal to approximately −0.41+i0.41 and 0.33+i0.31 for the pump and probe wavelengths, respectively [19]. The values of the higher-order susceptibilities at the pump and probe wavelengths are assumed to be the same as those at the ENZ wavelength (1240 nm). This assumption is based on the experimental results in the literature [19,22,23].

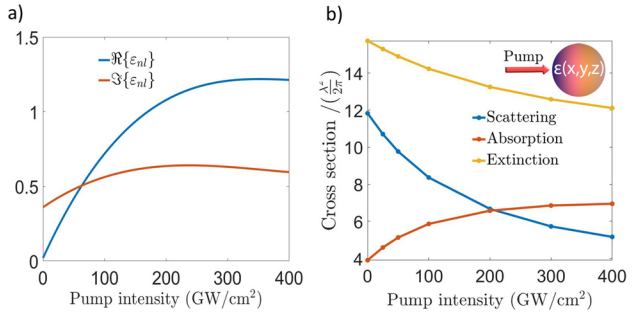

Fig. 2. (a) Pump intensity dependent real and imaginary parts of ITO's permittivity at the ENZ wavelength (1240 nm). (b) Pump intensity dependent scattering, absorption, and extinction cross sections of the ITO sphere at the pump wavelength. The inset figure shows a visual illustration of the setup.

A recursive simulation based on a frequency-domain finite-element full-wave Maxwell solver is used to calculate the steady-state inhomogeneous permittivity induced by the pump. We recursively update the electric field and permittivity value simultaneously at each point in space until the steady-state value is reached. Each iteration requires a finite-element simulation to calculate the electric field based on the permittivity values computed from the previous iteration. Next, the permittivity is recomputed at each spatial point from the electric fields at each point using Eq. (1), and the process is repeated until convergence.

Figure 2(b) shows the scattering, absorption, and extinction cross sections for the optical pump. The sphere's radius is always 700 nm. The normalized scattering cross section of the pump decreases from approximately 12 to 5 by increasing the optical pump intensity. Similarly, the absorption and extinction cross sections of the pump can be tuned by changing the optical pump intensity. This change in the cross sections is physically intuitive due to the intensity-dependent permittivity. More quantitatively, Fig. 3 shows the real and imaginary parts of the permittivity in different YZ-, XZ-, and XY-planes at the probe wavelength using an optical pump intensity of 200 GW/cm^2. The real and imaginary parts of the permittivity are symmetric along the x and y axes. They gradually change from 0.35 to 1.45 and from 0.4 to 0.6, respectively, along the propagation direction of the incident pump wave (the Z-direction). This symmetry along the x and y axes is approximate and not exact because the optical pump is linearly polarized and thus the symmetry is broken.

Now, we study the interaction of a low-intensity probe with the pumped ITO sphere. We modify the illumination direction of the probe by choosing different spherical angles (ϕ and θ), shown in Fig. 4(a). First, we calculate the T-matrix of the sphere at the probe wavelength [25]. The T-matrix links the coefficients of the incident to the coefficients of the scattered field when expanded in a vector spherical harmonic (VSH) basis. To calculate the T-matrix, we study the scattering from the sphere when it is illuminated with an incident field corresponding to a specific VSH. Expanding the scattered field in the VSH basis provides one column of the T-matrix. The scattered field is calculated using a finite-element full-wave Maxwell solver. The space-dependent permittivity induced by the pump, as shown in Fig. 3, is considered as the sphere's permittivity. The process repeats with multiple VSH to retrieve all columns of the T-matrix.

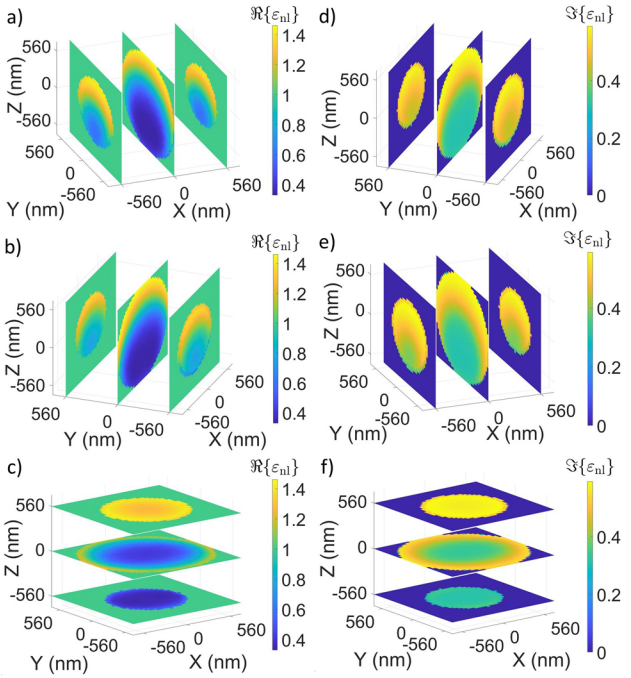

Fig. 3. (a)–(c) Real and (d)–(f) imaginary part of the permittivity in different planes for a sphere, pumped with an intensity of 200 GW/cm^2 at the probe wavelength (1180 nm). The incident pump is an x-polarized plane wave at a wavelength of 1300 nm that propagates in the z-direction.

The T-matrix is truncated to a fifth multipolar order:

$$\begin{bmatrix} \mathbf{b}_1^{\mathrm{e}} \\ \vdots \\ \mathbf{b}_5^{\mathrm{e}} \\ \mathbf{b}_1^{\mathrm{m}} \\ \vdots \\ \mathbf{b}_5^{\mathrm{m}} \end{bmatrix} = \begin{bmatrix} \overline{\overline{T_{11}^{\mathrm{ee}}}} & \cdots & \overline{\overline{T_{15}^{\mathrm{ee}}}} & \overline{\overline{T_{11}^{\mathrm{em}}}} & \cdots & \overline{\overline{T_{15}^{\mathrm{em}}}} \\ \vdots & & \vdots & \vdots & & \vdots \\ \overline{\overline{T_{51}^{\mathrm{ee}}}} & \cdots & \overline{\overline{T_{55}^{\mathrm{ee}}}} & \overline{\overline{T_{51}^{\mathrm{em}}}} & \cdots & \overline{\overline{T_{55}^{\mathrm{em}}}} \\ \overline{\overline{T_{11}^{\mathrm{me}}}} & \cdots & \overline{\overline{T_{15}^{\mathrm{me}}}} & \overline{\overline{T_{11}^{\mathrm{mm}}}} & \cdots & \overline{\overline{T_{15}^{\mathrm{mm}}}} \\ \vdots & & \vdots & \vdots & & \vdots \\ \overline{\overline{T_{51}^{\mathrm{me}}}} & \cdots & \overline{\overline{T_{55}^{\mathrm{me}}}} & \overline{\overline{T_{51}^{\mathrm{mm}}}} & \cdots & \overline{\overline{T_{55}^{\mathrm{mm}}}} \end{bmatrix} \begin{bmatrix} \mathbf{q}_1^{\mathrm{e}} \\ \vdots \\ \mathbf{q}_5^{\mathrm{e}} \\ \mathbf{q}_1^{\mathrm{m}} \\ \vdots \\ \mathbf{q}_5^{\mathrm{m}} \end{bmatrix}, \quad \textbf{(2)}$$

where $\mathbf{b}_i^{\mathrm{e}}$ ($\mathbf{b}_i^{\mathrm{m}}$), and $\mathbf{q}_j^{\mathrm{e}}$ ($\mathbf{q}_j^{\mathrm{m}}$) denote the ith and jth components of the scattered and incident electric (magnetic) field, respectively, in a VSH basis [25]. Here, $\mathbf{b}_j^{\mathrm{v}}$ and $\mathbf{q}_j^{\mathrm{v}}$ are equal to $[b_{j,-j}^{v} b_{j,-j+1}^{v} \cdots b_{j,j-1}^{v} b_{j,j}^{v}]$, and $[q_{j,-j}^{v} q_{j,-j+1}^{v} \cdots q_{j,j-1}^{v} q_{j,j}^{v}]$, respectively, where j refers to the multipolar order (max. 5), and v = $\{e, m\}$ denotes the multipolar type [electric (e), or magnetic (m)] [26]. Additionally, $\overline{\overline{\mathrm{T}_{\mathrm{ij}}^{\mathrm{ee}}}}$, $\overline{\overline{\mathrm{T}_{\mathrm{ij}}^{\mathrm{mm}}}}$, $\overline{\overline{\mathrm{T}_{\mathrm{ij}}^{\mathrm{em}}}}$, and $\overline{\overline{\mathrm{T}_{\mathrm{ij}}^{\mathrm{me}}}}$ refer to the sub-matrices that quantify the electric-electric, magnetic-magnetic, electric-magnetic, and magnetic-electric response, respectively, between the ith scattered field VSH, and the jth incident field VSH [26].

We focus on two extreme values of the optical pump intensity: 0.01 and 200 GW/cm^2 corresponding to the linear and highly nonlinear regimes. In the linear regime, shown in Fig. 4(b), all the non-zero elements of the T-matrix lie on the diagonal of the matrix (in the electric-electric and magnetic-magnetic parts). The sphere exhibits an isotropic response without any electromagnetic coupling. In contrast, in the highly nonlinear case, shown in Fig. 4(c), some of the off diagonal elements, which quantify the electromagnetic and magnetoelectric coupling, are non-zero. More specifically, the absolute values of the

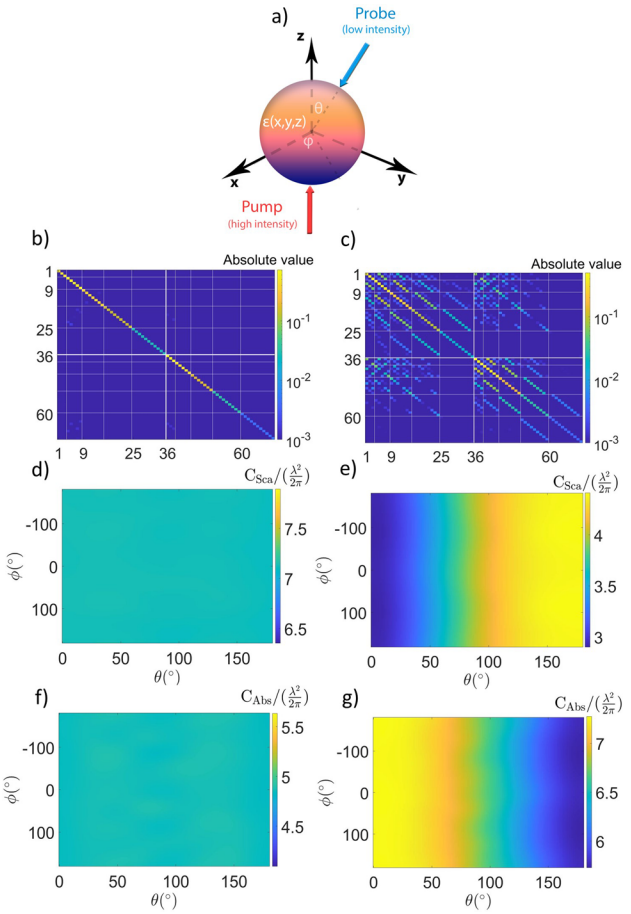

Fig. 4. (a) Setup for an optical pump–probe beam impinging on an ITO sphere. (b), (c) Absolute values of the T-matrix elements with an expansion order of 5 for optical pump intensities of 0.01 GW/cm^2 and 200 GW/cm^2, corresponding to linear and highly nonlinear regime, respectively. (d), (e) Scattering cross section at the probe wavelength (1180 nm) in the linear and highly nonlinear regime depending on the spherical angles (θ and ϕ). (f), (g) Absorption cross section in the linear and highly nonlinear regimes, respectively.

T-matrix coefficients for the electro-magnetic and the magneto-electric coefficients have a maximum value of 0.06, while the maximum absolute value of the T-matrix coefficients for the electric-electric and the magnetic-magnetic parts is roughly 0.5. The appearance of the off diagonal elements confirms the bianisotropic response of the ITO sphere in the nonlinear regime. Based on the intensity of the optical pump, an isotropic sphere is converted to a bianisotropic one, where the bianisotropic response of the probe can be tuned and controlled using the external pump.

To explore the potential, we calculate the extinction, scattering, and absorption cross sections of the ITO sphere probed at different angles. The cross sections are calculated as [25]

$$C_{\mathrm{ext}} = -\frac{1}{k^2 |\mathbf{E}_0^{\mathrm{inc}}|^2} \sum_{j=1}^{5} \Re\left(\mathbf{q}_j^{\mathrm{e,T}} \mathbf{b}_j^{e,*} + \mathbf{q}_j^{\mathrm{m,T}} \mathbf{b}_j^{\mathrm{m},*}\right), \quad \textbf{(3)}$$

$$C_{\mathrm{sca}} = \frac{1}{k^2 |\mathbf{E}_0^{\mathrm{inc}}|^2} \sum_{j=1}^{5} \left(|\mathbf{b}_j^{\mathrm{e}}|^2 + |\mathbf{b}_j^{\mathrm{m}}|^2\right), \quad \textbf{(4)}$$

$$C_{\mathrm{abs}} = C_{\mathrm{ext}} - C_{\mathrm{sca}}, \quad \textbf{(5)}$$

where $\mathbf{E}_0^{\text{inc}}$ and k are the incident electric field of the probe and its wavenumber. Here, T and $*$ refer to the transpose and complex conjugation operations. The probe scattering cross section is shown in Figs. 4(d) and 4(e) for the low and high optical-pump intensity cases, using a probe plane wave with a transverse magnetic polarization. The scattering cross section is the same for different propagation directions of the probe beam in the linear regime. For high optical pump intensities, the scattering cross section increases approximately from 2.9 to 4.4 when θ changes from 0 to 180°. Reciprocity is assured since the pumped sphere is equivalent to an inhomogeneous lossy dielectric material. Hence, the extinction cross sections are the same for every pair of opposite directions. Based on this principle, the absorption cross section is calculated in Figs. 4(f) and 4(g) for the low and high optical-pump intensities. Analogous to the scattering cross section, the absorption cross sections are identical regardless of the probe direction for low pump intensities. However, they decrease from 7.2 to 5.8 when θ changes from 0 to 180° at high pump intensities. The observation confirms that a high-intensity optical pump transforms an isotropic sphere into a structure with angle-dependent scattering and absorption cross sections.

Nanoparticles made of materials such as GaAs, Si, or other traditional optical materials in certain wavelength regimes possess large absorption coefficients, which may result in a large local intensity gradient. However, the feasible modulation index in these materials is orders of magnitude smaller than what is possible in ITO at the ENZ wavelengths due to their high base indices [27]. In contrast, phase change materials such as vanadium dioxide exhibit large changes in permittivities associated with metal–dielectric phase transition [28–30]. However, since the phase transition in such a material is dictated by temperature, a strong temperature gradient is necessary to observe light-induced bianisotropy. Thus, it is not obvious how heat transport can be obstructed in a vanadium dioxide nanoparticle to demonstrate tunable and reversible light-induced bianisotropy. Hence, we posit that ITO and similar ENZ materials are perhaps most suited for experimental demonstration of the introduced concept.

In conclusion, we discussed a novel concept to obtain a tunable bianisotropic response in a nonlinear antenna. Using ITO as the nonlinear material, one can tune the response of the antenna at sub-picoseconds scales. The idea is general and can be implemented with any medium with a strong nonlinear response. This concept is expected to open the door for further studies to create novel metasurfaces that rely on tunable bianisotropy. Such structures could address diverse applications in photonics, such as tunable dispersion and absorption. Our scheme benefits from this additionally introduced extra degree of freedom to control and manipulate the electromagnetic waves in different media and structures, based on the optical pump characteristics.

Funding. Erasmus+; Alexander von Humboldt-Stiftung; Helmholtz Association; Karlsruhe Institute of Technology; Natural Sciences and Engineering Research Council of Canada; Canada Excellence Research Chairs, Government of Canada; Canada First Research Excellence Fund.

Acknowledgments. M.A.A.A. acknowledges funding through the Erasmus EUROPHOTONICS M.Sc. program. R.A. acknowledges the support of the Alexander von Humboldt Foundation through the Feodor Lynen Fellowship. R.A., MZ.A., and R.W.B. acknowledge support through the Natural Sciences and Engineering Research Council of Canada, the Canada Research Chairs program, and the Canada First Research Excellence Fund.

Disclosures. The authors declare no conflicts of interest.

Data availability. Data underlying the results presented in this paper are not publicly available at this time but may be obtained from the authors upon reasonable request.

REFERENCES

1. Y. Ra'di, V. S. Asadchy, and S. A. Tretyakov, IEEE Trans. Antennas Propagat. **62**, 3749 (2014).
2. C. Pfeiffer and A. Grbic, Phys. Rev. Appl. **2**, 044011 (2014).
3. C. Pfeiffer, C. Zhang, V. Ray, L. J. Guo, and A. Grbic, Phys. Rev. Lett. **113**, 023902 (2014).
4. V. S. Asadchy, A. Díaz-Rubio, and S. A. Tretyakov, Nanophotonics **7**, 1069 (2018).
5. S. Tretyakov, F. Mariotte, C. Simovski, T. Kharina, and J.-P. Heliot, IEEE Trans. Antennas Propagat. **44**, 1006 (1996).
6. T. G. Mackay and A. Lakhtakia, *Electromagnetic Anisotropy and Bianisotropy: a Field Guide* (World Scientific, 2010).
7. R. Alaee, M. Albooyeh, M. Yazdi, N. Komjani, C. Simovski, F. Lederer, and C. Rockstuhl, Phys. Rev. B **91**, 115119 (2015).
8. R. Alaee, M. Albooyeh, A. Rahimzadegan, M. S. Mirmoosa, Y. S. Kivshar, and C. Rockstuhl, Phys. Rev. B **92**, 245130 (2015).
9. D. Jalas, A. Petrov, M. Eich, W. Freude, S. Fan, Z. Yu, R. Baets, M. Popović, A. Melloni, J. D. Joannopoulos, M. Vanwolleghem, C. R. Doerr, and H. Renner, Nat. Photonics **7**, 579 (2013).
10. A. M. Mahmoud, A. R. Davoyan, and N. Engheta, Nat. Commun. **6**, 8359 (2015).
11. S. A. Tretyakov, Microw. Opt. Technol. Lett. **19**, 365 (1998).
12. Y. Shoji, M. Ito, Y. Shirato, and T. Mizumoto, Opt. Express **20**, 18440 (2012).
13. Y. Zongfu and F. Shanhui, Nat. Photonics **3**, 91 (2009).
14. M. Li, Y. Hu, Q. Chen, H. Chen, and Z. Wang, New J. Phys. **23**, 085002 (2021).
15. K. Fan, A. C. Strikwerda, X. Zhang, and R. D. Averitt, Phys. Rev. B **87**, 161104 (2013).
16. Y. Moritake and T. Tanaka, Sci. Rep. **7**, 6726 (2017).
17. Y. Moritake and T. Tanaka, Sci. Rep. **8**, 9012 (2018).
18. D. Tzarouchis and A. Sihvola, Appl. Sci. **8**, 184 (2018).
19. M. Z. Alam, I. De Leon, and R. W. Boyd, Science **352**, 795 (2016).
20. I. Liberal and N. Engheta, Science **358**, 1540 (2017).
21. O. Reshef, I. De Leon, M. Z. Alam, and R. W. Boyd, Nat. Rev. Mater. **4**, 535 (2019).
22. H. Wang, K. Du, C. Jiang, Z. Yang, L. Ren, W. Zhang, S. J. Chua, and T. Mei, Phys. Rev. Appl. **11**, 064062 (2019).
23. O. Reshef, E. Giese, M. Z. Alam, I. De Leon, J. Upham, and R. W. Boyd, Opt. Lett. **42**, 3225 (2017).
24. R. W. Boyd, *Nonlinear Optics* (Academic Press, 2020).
25. M. I. Mishchenko, L. D. Travis, and A. A. Lacis, *Scattering, Absorption, and Emission of Light by Small Particles* (Cambridge University Press, 2002).
26. A. Rahimzadegan, T. D. Karamanos, R. Alaee, A. G. Lamprianidis, D. Beutel, R. W. Boyd, and C. Rockstuhl, Adv. Opt. Mater. **10**, 2102059 (2022).
27. S. Benis, N. Munera, S. Faryadras, E. W. V. Stryland, and D. J. Hagan, Opt. Mater. Express **12**, 3856 (2022).
28. A. Howes, Z. Zhu, D. Curie, J. R. Avila, V. D. Wheeler, R. F. Haglund, and J. G. Valentine, Nano Lett. **20**, 4638 (2020).
29. A. Howes, W. Wang, I. Kravchenko, and J. Valentine, Optica **5**, 787 (2018).
30. I. O. Oguntoye, A. J. Ollanik, S. Padmanabha, G. Z. Hartfield, B. K. Simone, and M. D. Escarra, *CLEO: QELS_Fundamental Science* (Optical Society of America, 2020), paper FTh3Q–1.